JACS
JOURNAL OF THE AMERICAN CHEMICAL SOCIETY
Article
pubs.acs.org/JACS

Kinetic Analysis of Competitive Electrocatalytic Pathways: New Insights into Hydrogen Production with Nickel Electrocatalysts

Eric S. Wiedner,* Houston J. S. Brown, and Monte L. Helm

Center for Molecular Electrocatalysis, Pacific Northwest National Laboratory, P.O. Box 999, K2-57, Richland, Washington 99352, United States

Supporting Information

ABSTRACT: The hydrogen production electrocatalyst $Ni(P^{Ph}_2N^{Ph}_2)_2^{2+}$ (**1**) is capable of traversing multiple electrocatalytic pathways. When using dimethylformamidium, $DMF(H)^+$, the mechanism of H_2 formation by **1** changes from an ECEC to an EECC mechanism as the potential approaches the Ni(I/0) couple. Two electrochemical methods, current−potential analysis and foot-of-the-wave analysis (FOWA), were performed on **1** to measure detailed kinetics of the competing ECEC and EECC pathways. A sensitivity analysis was performed on the methods using digital simulations to understand their strengths and limitations. Chemical rate constants were significantly underestimated when not accounting for electron-transfer kinetics, even when electron transfer was fast enough to afford a reversible noncatalytic wave. The EECC pathway of **1** was faster than the ECEC pathway under all conditions studied. Buffered DMF:$DMF(H)^+$ mixtures afforded an increase in the catalytic rate constant (k_{obs}) of the EECC pathway, but k_{obs} for the ECEC pathway did not change when using buffered acid. Further kinetic analysis of the ECEC path revealed that base increases the rate of isomerization from exo-protonated Ni(0) isomers to the catalytically active endo-isomers, but decreases the rate of protonation of Ni(I). FOWA did not provide accurate rate constants, but FOWA was used to estimate the reduction potential of the previously undetected exo-protonated Ni(I) intermediate. Comparison of catalytic Tafel plots for **1** under different conditions reveals substantial inaccuracies in the turnover frequency at zero overpotential when the kinetic and thermodynamic effects of the conjugate base are not accounted for properly.

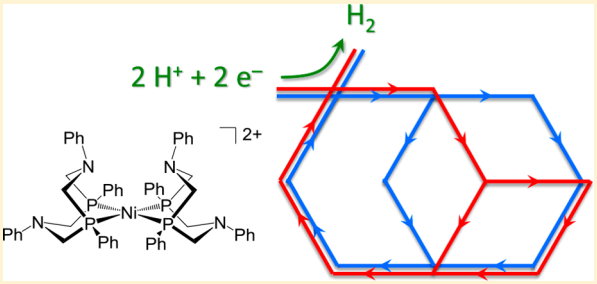

INTRODUCTION

Replacing fossil fuels with energy generated from renewable sources, coupled with the desire to use energy more efficiently, has driven a resurgence in research and development of electrocatalysts for energy storage and use.[1] A wide variety of molecular complexes have been studied as electrocatalysts for production of H_2 and reduction of CO_2.[2−6] Enabling the rational design and improvement of molecular electrocatalysts requires careful mechanistic studies to determine key catalytic intermediates and kinetic bottlenecks.

Electrocatalytic cyclic voltammetry has become an indispensable tool for understanding overall rates of molecular catalysis, overpotential, and catalytic mechanisms.[7,8] A seminal report by Costentin and Savéant in 2014 provides the groundwork for detailed kinetic analysis of multi-electron electrocatalysis by molecular compounds.[9,10] In electrochemical nomenclature, electron transfers and chemical steps are denoted as "E" and "C", respectively. From an electrochemical perspective, electrocatalytic H_2 production can be simplified into two proton-transfer steps (C) and two electron-transfer steps (E), which can occur in five possible orders: ECEC, EECC, ECCE, CECE, and CCEE. Costentin and Savéant provided a current−potential analysis for each the three mechanisms that begin with an electron-transfer step,[9] allowing for determination of the rate constant for each chemical step without the use of digital simulation software.

As with digital simulation techniques, incorrect assignment of the catalytic mechanism can lead to misleading or incorrect kinetic information. This problem can be exacerbated if the catalyst is capable of traversing multiple competing pathways for catalytic turnover, as frequently observed with molecular complexes that catalyze the reduction of protons or CO_2.[11−21] The careful delineation of the possible relevant mechanisms, the methods and expressions for extracting the kinetic data, and sensitivity analysis of different electrochemical methods are crucial for thorough and accurate analysis of electrocatalytic data. Herein we report an electrochemical mechanistic analysis for proton reduction catalysis by the well-established $Ni(P^{Ph}_2N^{Ph}_2)_2^{2+}$ (**1**) complex[22−24] using the multi-electron, multichemical step analysis recently reported by Costentin and Savéant.[9] Using this catalyst, we present methods for analyzing competing ECEC and EECC catalytic pathways and evaluate the error associated with these methods.

RESULTS

Identification of Relevant Mechanisms. The reduction of protons to form H_2 using $Ni(P^{Ph}_2N^{Ph}_2)_2^{2+}$ (**1**) has been previously reported,[23−26] and mechanistic studies on $Ni(P^{R}_2N^{R'}_2)_2^{2+}$

Received: October 16, 2015
Published: December 21, 2015

DOI: 10.1021/jacs.5b10853
J. Am. Chem. Soc. 2016, 138, 604−616

derivatives have appeared in the literature.[22,27−29] As previously reported, cyclic voltammograms of **1** recorded in acetonitrile display two reversible waves corresponding to the Ni(II/I) couple (−0.83 V) and the Ni(I/0) couple (−1.03 V).[23,24] A representative cyclic voltammogram of **1** recorded in the presence of protonated dimethylformamide, $DMF(H)^+$, is shown in Figure 1. The wave approximates an ideal S-shaped catalytic

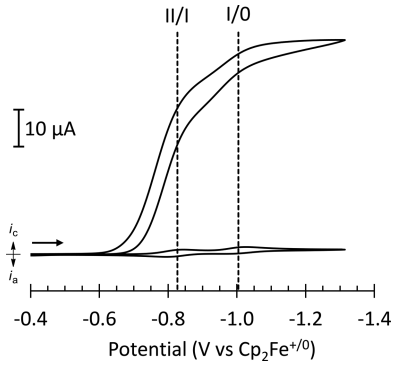

Figure 1. Cyclic voltammogram of **1** (0.7 mM) in the presence of $DMF(H)^+$ (158 mM) in MeCN (0.2 M NBu_4PF_6), showing the $E_{1/2}$ of the noncatalytic Ni(II/I) and Ni(I/0) couples relative to the catalytic wave. Conditions: υ = 0.05 V s^{-1}, 1 mm diameter glassy carbon working electrode.

wave, and the maximum catalytic current (i_{cat}) is independent of the scan rate employed. However, the catalytic wave also displays a discernible inflection point near −0.9 V, located approximately halfway between the Ni(II/I) and Ni(I/0) couples. This inflection is a deviation away from ideal electrocatalytic behavior and suggests a change in the catalytic mechanism as the potential is swept more negative.

The appearance of a single inflection point in the catalytic wave of **1** (Figure 1) suggests that the majority of the catalytic current stems from only two of the five possible E/C mechanisms for H_2 production. Several of the candidate mechanisms for catalysis by **1** can be reasonably excluded based on experimental observations and estimated pK_a values of the protonated pendant amines in the $Ni(P^{Ph}_2N^{Ph}_2)_2^{2+}$ complex relative to the pK_a of $DMF(H)^+$ in CH_3CN (6.1).[30,31] For $Ni(P^R_2N^{R'}_2)_2^{2+}$ complexes that can be protonated in the Ni(II) state, the catalytic half-wave potential is ∼350 mV more positive than the Ni(II/I) couple of the unprotonated complex.[32,33] The shift in $E_{cat/2}$ versus the Ni(II/I) couple of **1** is smaller than 200 mV, therefore the mechanisms involving protonation of Ni(II) before electrochemical reduction (CECE and CCEE) can be ruled out as major pathways. The ECCE mechanism can also be eliminated as protonation of a monoprotonated Ni(I) species by $DMF(H)^+$ is unlikely. Based on electrostatic arguments, the basicity of a protonated Ni(I) species (overall +2 charge) would be similar to that of a Ni(II) complex (overall +2 charge). These pK_a approximations are well supported by previous computational studies on the $Ni(P^R_2N^{R'}_2)_2^{2+}$ family of complexes.[34,35] The two remaining mechanistic candidates are the ECEC and EECC mechanisms, both of which are discussed below.

The non-ideal inflection in the catalytic wave of proton reduction by **1** can be attributed to either a change from an ECEC to an EECC mechanism or from two distinct ECEC mechanisms occurring at different potentials. For example, protonation of Ni(I) at a pendant amine can occur in either an endo or an exo position (Chart 1). If the reduction potentials of

Chart 1. Endo vs Exo Protonation Isomers of Ni(I)[a]

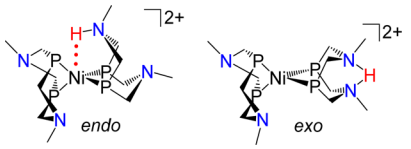

[a]The groups on P and N have been omitted for clarity.

the endo and exo protonated intermediates are sufficiently different, two catalytic waves corresponding to an ECEC mechanism could be observed. The protonated Ni(I) intermediates of **1** have not been observed previously, but comparison of **1** with related $Ni(P^R_2N^{R'}_2)_2^{2+}$ complexes suggests that the reduction potentials of both the endo and exo-protonated Ni(I) forms of **1** are more positive than the Ni(II/I) couple (see Discussion section for further details). Therefore, the observed inflection point in the electrocatalytic wave is most likely due to a change in mechanism from an initial ECEC mechanism to an EECC mechanism, both of which are depicted generically in Scheme 1 to show the overall

Scheme 1. Generalized ECEC and EECC Mechanisms for 1

ECEC:

$Ni(II)^{2+} + e^- \rightleftharpoons Ni(I)^+$	E_1
$Ni(I)^+ + H^+ \rightleftharpoons Ni(I)H^{2+}$	C_1
$Ni(I)H^{2+} + e^- \rightleftharpoons Ni(0)H^+$	E_2
$Ni(0)H^+ + H^+ \rightleftharpoons Ni(II)^{2+} + H_2$	C_2

EECC:

$Ni(II)^{2+} + e^- \rightleftharpoons Ni(I)^+$	E_1
$Ni(I)^+ + e^- \rightleftharpoons Ni(0)$	E_2
$Ni(0) + H^+ \rightleftharpoons Ni(0)H^+$	C_1
$Ni(0)H^+ + H^+ \rightleftharpoons Ni(II)^{2+} + H_2$	C_2

stoichiometry (and not structure or connectivity). For instance, $Ni(0)H^+$ could be either an exo-protonated Ni(0) complex, $Ni^0(P^{Ph}_2N^{Ph}_2\text{-}H)(P^{Ph}_2N^{Ph}_2)^+$, or a formal Ni(II)-hydride, $HNi^{II}(P^{Ph}_2N^{Ph}_2)_2^+$.

Defining the Kinetic Parameters. For a two-electron electrocatalytic process in which both electron transfers occur at the electrode, the maximum catalytic current (i_{cat}) is given by eq 1, where F is Faraday's constant, A is the area of the electrode in cm^2, $[Cat]_T$ is the concentration of catalyst, D is the diffusion coefficient in cm^2 s^{-1}, and k_{obs} is the observed catalytic rate constant in s^{-1}.[36−38] When a reversible noncatalytic wave can be observed in the absence of substrate, dividing eq 1 by the noncatalytic peak current (i_p) results in cancellation of A, $[Cat]_T$, and D, and the ratio i_{cat}/i_p becomes a function of k_{obs}, the scan rate (υ), and the electrochemical parameter f, which is equal to F/RT (eq 2). Eq 2 is readily rearranged to give eq 3, thus k_{obs} can be determined from the measured electrochemical parameters i_{cat} and i_p without prior knowledge of the specific two-electron catalytic mechanism.

$$i_{cat} = 2FA[Cat]_T\sqrt{D}\sqrt{k_{obs}} \quad (1)$$

$$\frac{i_{cat}}{i_p} = 4.48\sqrt{\frac{k_{obs}}{f\upsilon}} \quad (2)$$

DOI: 10.1021/jacs.5b10853
J. Am. Chem. Soc. 2016, 138, 604−616

Table 1. Kinetic Parameters for ECEC and EECC Mechanisms

mechanism	$\sqrt{k_{obs}}$ ($s^{-1/2}$)[a]	λ[a]	k_1 (s^{-1})[b]	k_2 (s^{-1})[b]
ECEC[c]	$\frac{\sqrt{k_1}}{1+\lambda}$	$\frac{\sqrt{k_1}}{\sqrt{k_2}}$	$k_{obs}(1+\lambda)^2$	$\frac{k_1}{\lambda^2}$
EECC	$\frac{\sqrt{k_1}}{1+\lambda}$	$\frac{\sqrt{k_1}}{\sqrt{k_2}\left(1+\frac{\sqrt{k_2}}{\sqrt{k_1}}\right)}$	$k_{obs}(1+\lambda)^2$	$\left(\frac{1}{\lambda}-\frac{1}{2}\sqrt{\frac{4+\lambda}{\lambda}}+\frac{1}{2}\right)k_1$

[a]Reported in ref 9. [b]Derived from $\sqrt{k_{obs}}$ and λ (see the SI). [c]For the case in which the second electron transfer is easier than the first electron transfer ($E_1 < E_2$ for a reduction). A different set of $\sqrt{k_{obs}}$ and λ are obtained for an ECEC mechanism in which the second electron transfer is more difficult than the first ($E_1 > E_2$).[9]

$$k_{obs} = 0.0497 f v \left(\frac{i_{cat}}{i_p}\right)^2 \quad (3)$$

Costentin and Savéant recently described the dependence of k_{obs} on k_1 and k_2, the rate constants for the two individual chemical steps (C), in the ECEC, EECC and ECCE mechanisms.[9] Additionally, they described the potential at half-height of the catalytic wave ($E_{cat/2}$) according to eq 4, where $E_{1/2}$ is the half-wave potential of the reversible noncatalytic wave and λ is a mechanism-dependent kinetic parameter.[9] Eq 4 can be rearranged to give eq 5, thus λ can be determined directly from the measured $E_{1/2}$ and $E_{cat/2}$ values.

$$E_{cat/2} = E_{1/2} + \frac{1}{f}\ln(1+\lambda) \quad (4)$$

$$\lambda = \exp[f(E_{cat/2} - E_{1/2})] - 1 \quad (5)$$

Determination of λ allows for calculation of the two individual chemical step rate constants, k_1 and k_2 in terms of experimental observables. Table 1 gives the expressions for $\sqrt{k_{obs}}$ and λ in terms of k_1 and k_2 (expressed as pseudo-first-order rate constants, e.g., $k_1 = k_1'[HA]$) for ECEC and EECC mechanisms in which the second electron transfer is easier than the first ($E_1 < E_2$). These expressions are obtained from algebraic rearrangement of the reported equations.[9] As seen in Table 1, the ECEC and EECC mechanisms possess the same general form of $\sqrt{k_{obs}}$, but differ in the form of λ. After algebraic manipulation, k_1 can be expressed in terms of the experimental measurables, k_{obs} and λ, and similarly k_2 can be expressed in terms of and k_1 and λ (see Supporting Information (SI) for derivations).

A common approximation in multistep electrocatalytic mechanisms is that k_{obs} corresponds to a single rate-limiting step in the catalytic cycle. The dependence of k_{obs} on the values of k_1 and k_2 reveals that this assumption is only valid when the rates for the two steps differ by several orders of magnitude and that the precise relationship depends on the mechanism. For example, this relationship is illustrated for the kinetic regime of $k_1 \geq k_2$ in Figure 2, where k_{obs}/k_2 expresses the relationship between the catalytic rate (k_{obs}) and the slow step (k_2) as a function of $\log(k_1/k_2)$, which defines the relative magnitude of the two individual rate constants. For an ECEC mechanism (red trace), k_{obs} will not be equivalent to k_2 until $\log(k_1/k_2) \geq 4$, i.e., the first step is at least 4 orders of magnitude faster than the second step. The kinetics are different for an EECC mechanism (blue trace), where k_{obs} becomes equivalent to k_2 at a much smaller value of $\log(k_1/k_2) \sim 2$. These examples illustrate the importance of understanding the catalytic mechanism and

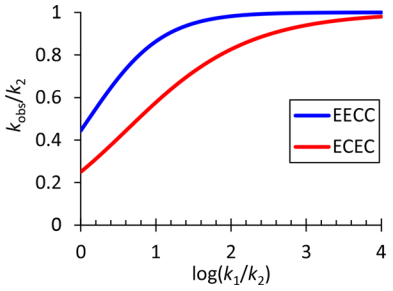

Figure 2. Plot of k_{obs}/k_2 versus $\log(k_1/k_2)$ for ECEC and EECC mechanisms.

relationship between the rate constants for the elementary reaction steps before drawing general conclusions about rate-determining steps from the overall rate constant, k_{obs}. In situations where both k_1 and k_2 contribute to k_{obs}, it is important to be able to measure the individual rate constants to gain insight into how to improve catalytic bottlenecks.

Before analyzing catalytic data to determine the individual k_1 and k_2 rate constants, it is important to understand the assumptions and limitations of the equations in Table 1. One important assumption in the derivation of the expressions for λ in Table 1 is that electron transfer from the electrode to the catalyst is fast enough to obey the Nernst law.[9] The limitations of this assumption do not appear to have been tested in the literature, and electron-transfer kinetics might be especially important for very fast catalysts (i.e., $k_{obs} > 100\ s^{-1}$). To demonstrate how the catalytic response might be affected, the Butler–Volmer model of electron transfer (eq 6) is considered:

$$k_f = k_s \exp[-\alpha f(E - E_{1/2})] \quad (6)$$

where k_f is the forward rate constant for reduction by the electrode ($cm\ s^{-1}$), k_s is the standard heterogeneous electron-transfer rate constant ($cm\ s^{-1}$), and α is the transfer coefficient ($0 \leq \alpha \leq 1$), a unitless term that describes the symmetry of the energy barrier for electron transfer ($\alpha = 0.5$ for a perfectly symmetrical barrier).[10,39] At the plateau of a catalytic wave, the applied potential (E) is negative of $E_{1/2}$, and k_f will be large. However, k_f will be much smaller at potentials positive of $E_{1/2}$, such as at $E_{cat/2}$. Eq 4 describing $E_{cat/2}$ can only be rigorously correct if k_f is large enough to generate the reduced catalyst (e.g., Ni(I) in the case of **1**) faster than it is consumed in the catalytic cycle, thus requiring large values of k_s.

Digital simulation was employed to test the effect of k_s on the value of k_1 calculated from k_{obs} and λ. A reversible, $1e^-$ reduction wave was simulated with values of k_s ranging from 100 to 0.01 $cm\ s^{-1}$ (for reference, ferrocene has been reported[40] to have $k_s = 0.25\ cm\ s^{-1}$ relative to a glassy carbon electrode in

DOI: 10.1021/jacs.5b10853
J. Am. Chem. Soc. 2016, 138, 604–616

acetonitrile). Next, the noncatalytic reduction wave was simulated as a catalytic ECEC mechanism with k_2 arbitrarily chosen to be 100 s^{-1} and variable values of k_1 such that $k_1 \geq k_2$. The apparent k_1 value was then determined from i_{cat}/i_p and $E_{cat/2}$ of the simulated voltammograms using different values for k_s. The accuracy of the k_1 measurement was evaluated from the percent error relative to the value used in the simulation. Figure 3 shows a plot of % error versus log(k_s), with negative

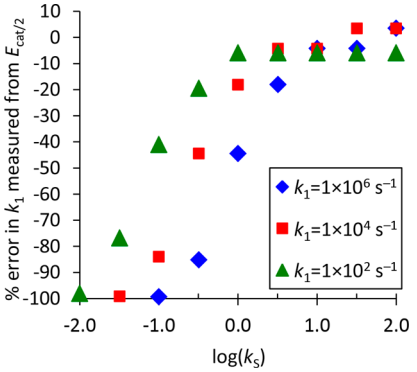

Figure 3. Plot of % error in k_1 measured from $E_{cat/2}$ versus log(k_s) at different values of k_1. ECEC model: $E_1 - E_2 = -0.5$ V, $k_2 = 100$ s^{-1}, $\upsilon = 0.05$ V s^{-1}, $D = 1 \times 10^{-5}$ cm^2 s^{-1}.

error values corresponding to an underestimation of k_1. For a very large value of $k_1 = 1 \times 10^6$ s^{-1} (blue diamonds), an error of −20% was measured at $k_s = 3.2$ cm s^{-1}, and further decreases in k_s cause a rapid drop in the accuracy; at $k_s = 0.1$ cm s^{-1}, an error of −99% was obtained, corresponding to an underestimation of two orders of magnitude for k_1. Similar trends are observed for smaller values of k_1 (red and green traces), except that the decrease in accuracy begins at smaller values of k_s. For example, for $k_1 = 100$ s^{-1} (green triangles), errors of <−10% are only observed at $k_s < 1.0$ cm s^{-1}. Using the k_s of ferrocene as a benchmark, catalysts that operate at $k_{obs} \geq 100$ s^{-1} and have electron-transfer rates slower than that of ferrocene (<0.25 cm s^{-1}, or log(k_s) = −0.6) will result in an underestimation of the calculated values of k_1 using the equations in Table 1.

Eq 4 can be modified to account for heterogeneous electron-transfer kinetics,[5,9,41] which would allow determination of λ from $E_{cat/2}$ after independent measurement of k_s and α. However, accurate measurement of k_s values in non-aqueous solvents presents a variety of experimental challenges.[42] In particular, a simple and popular voltammetric method for measuring k_s values is to measure the increase in the peak-to-peak separation of a redox wave at high scan rates.[43,44] The major challenge of this technique is to completely compensate for the solution resistance, which also causes the peak-to-peak separation to increase at high scan rates due to ohmic potential drop.[44] As an example, the value of k_s that is obtained for the $Cp_2Fe^{+/0}$ couple in acetonitrile relative to a glassy carbon electrode is much smaller when measured by cyclic voltammetry with iR compensation ($k_s = 0.009$ cm s^{-1})[45] than by AC voltammetry techniques ($k_s \cong 0.25$–0.5 cm s^{-1}).[40] Additionally, most studies of homogeneous electrocatalysts for proton reduction are performed using a glassy carbon electrode due to its large over-potential for acid reduction,[46,47] yet k_s values measured at glassy carbon electrodes have been shown to be highly sensitive to the surface microstructure[48,49] and polishing history.[50] Given the above considerations, experimental measurements of k_s values for molecular electrocatalysts are likely underestimated. With regard to determining chemical rate constants, an underestimate of k_s will lead to an overcorrection of $E_{cat/2}$, which will afford an overestimate of k_1 when $E_{cat/2}$ occurs positive of $E^{\circ\prime}$.

Foot-of-the-Wave Analysis. Foot-of-the-Wave analysis (FOWA) has been reported as a method for obtaining kinetic information on catalysts for which a plateau-shaped catalytic wave cannot be obtained due to competing side phenomena, such as substrate depletion or catalyst decomposition.[41,51,52] In general, a catalytic wave normalized to i_p can be described in terms of eq 7:

$$\frac{i}{i_p} = \frac{i_{cat}/i_p}{1 + \exp[f(E - E_{1/2})]} \quad (7)$$

In eq 7, the function $1/\{1 + \exp[f(E - E_{1/2})]\}$ describes the fraction of catalyst that is reduced at a given potential under noncatalytic conditions. For example, $1/\{1 + \exp[f(E - E_{1/2})]\}$ has a value of 0.5 at $E = E_{1/2}$, indicating half of the catalyst is reduced at the formal reduction potential. When the applied potential becomes more negative than $E_{1/2}$, the exponential term approaches 0 and eq 7 simplifies to eq 3. In FOWA, the normalized catalytic current (i/i_p) is plotted versus $1/\{1 + \exp[f(E - E_{1/2})]\}$, and the shape of the resulting plot depends on the kinetic regime of catalysis, as illustrated next.

Simulations were performed for several ECEC models, each having $k_{obs} = 100$ s^{-1} and different values of the kinetic parameter λ (recall that $\lambda = \sqrt{k_1/k_2}$ for the ECEC mechanism). In the first model, k_1 is much smaller than k_2 such that $\lambda = 0.01$, resulting in a catalytic wave having $E_{cat/2}$ equal to $E_{1/2}$ of the noncatalytic wave (Figure 4A, black trace). FOWA on this model affords a straight line with a slope (m) that is equal to i_{cat}/i_p (Figure 4B, black trace), thus providing access to k_{obs} (which is equal to k_1 in this kinetic regime) according to eq 3.

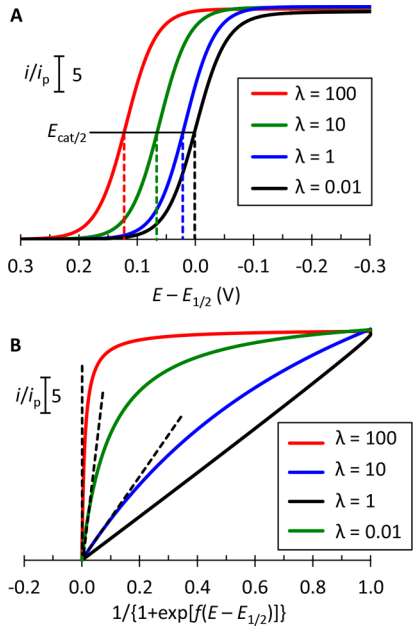

Figure 4. Plot of i/i_p versus $E - E_{1/2}$ (A) and $1/\{1 + \exp[f(E - E_{1/2})]\}$ (B) for ECEC mechanisms having $k_{obs} = 100$ s^{-1} but different values of k_1 and k_2. General ECEC model: $E_1 - E_2 = -0.5$ V, $k_s = 1 \times 10^4$ cm s^{-1}, $\upsilon = 0.05$ V s^{-1}, $D = 1 \times 10^{-5}$ cm^2 s^{-1}; red trace ($\lambda = 100$): $k_1 = 1 \times 10^6$ s^{-1}, $k_2 = 100$ s^{-1}; green trace ($\lambda = 10$): $k_1 = 1.2 \times 10^4$ s^{-1}, $k_2 = 120$ s^{-1}; blue trace ($\lambda = 1$): $k_1 = k_2 = 400$ s^{-1}; and black trace ($\lambda = 0.01$): $k_1 = 100$ s^{-1}, $k_2 = 1 \times 10^6$ s^{-1}.

DOI: 10.1021/jacs.5b10853
J. Am. Chem. Soc. 2016, 138, 604–616

Note that in this kinetic regime, k_2 cannot be measured from the catalytic wave since it occurs after the rate-determining step of the catalytic cycle.

When k_1 is no longer the sole rate-determining step, $E_{cat/2}$ becomes more positive than $E_{1/2}$, as shown in Figure 4a for ECEC models having $k_1 = k_2$ ($\lambda = 1$, blue trace) and $k_1 > k_2$ ($\lambda = 10$, green trace; $\lambda = 100$, red trace). FOWA plots of these waves are nonlinear, with the amount of curvature increasing as λ increases (Figure 4b). This phenomenon is best understood through expansion of the i_{cat}/i_p term in eq 7, providing eq 8 for an ECEC model, as shown below. At the foot of the wave, i.e., positive values of $E - E_{1/2}$, the term $\exp[f(E - E_{1/2})]$ is much larger than λ. Consequently, kinetic data on k_1 (the fast chemical step) can be obtained from the linear slope measured at the foot-of-the-wave (m_F) according to eq 9,[9] illustrated by the dashed traces in Figure 4b. As the potential is swept through the catalytic wave, $\exp[f(E - E_{1/2})]$ becomes smaller than λ, and eq 8 simplifies to eq 2 for i_{cat}/i_p. Similar FOWA plots are obtained for other mechanisms, such as EECC, when $k_1 \geq k_2$.

$$\frac{i}{i_p} = \frac{\frac{4.48}{\sqrt{f\upsilon}}\sqrt{k_1}}{\{1 + \lambda\}\{1 + \exp[f(E - E_{1/2})]\}} \quad (8)$$

$$m_F \cong 4.48\sqrt{\frac{k_1}{f\upsilon}} \quad (9)$$

A consideration that has not been clearly addressed in the literature is how much of the catalytic wave should be used in FOWA when the idealized FOWA plot is nonlinear. This was tested for the simulated ECEC model in the "fast k_1" regime (i.e., $E_{cat/2} > E_{1/2}$) using $k_2 = 100$ s^{-1}, several different values of k_1, and fast electron transfer ($k_s = 1 \times 10^4$ cm s^{-1}). The accuracy of the measured k_1 values was described by the percent error and was plotted against the fraction of i_{cat}/i_p used in the FOWA (Figure 5A). An error of approximately −5 to −13% was measured using only 3% of i_{cat}/i_p in the FOWA, and the error in k_1 clearly increases as more of the catalytic wave is employed in the FOWA. The analysis was repeated on the same model using a slower electron-transfer rate constant of $k_s = 0.1$ cm s^{-1} (Figure 5B). In this case, the inaccuracies in the measured k_1 become even greater as more of the foot is utilized, as expected given the effect of k_s on $E_{cat/2}$ determined above (Figure 3). However, utilizing only 3% of i_{cat}/i_p afforded an error of −20 to −30% for the measured k_1 values, which is much improved over the error of −40 to −84% obtained from the $E_{cat/2}$ analysis performed on the same catalytic waves (see Figure 3). While the specific errors in FOWA will depend on the values of k_s and the ratio k_1/k_2, these simulations demonstrate a clear benefit in using less of the catalytic wave in FOWA when a kinetic potential shift is observed.

The FOWA plots shown in Figure 4 bear a resemblance to FOWA plots obtained when either the substrate or catalyst is depleted within the diffusion layer.[8,51] Therefore, care should be taken to identify the correct rate constant being measured by FOWA, since accidental misrepresentation of k_1 as k_{obs} could lead to an overestimation of the catalytic rate. One possible way to confirm the kinetic regime is to substitute $E_{cat/2}$ for $E_{1/2}$ in the FOWA plot, i.e., a plot of i/i_p versus $1/\{1 + \exp[f(E - E_{cat/2})]\}$, which will afford a linear FOWA plot under all kinetic regimes. If $k_1 \geq k_2$, then the FOWA plot using $E_{cat/2}$ will give a smaller rate constant than the FOWA plot using $E_{1/2}$.

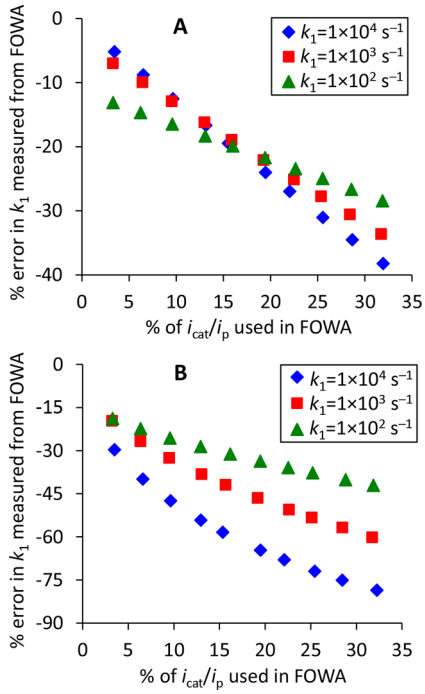

Figure 5. Plots of % error in k_1 measured from FOWA vs fraction of i_{cat}/i_p used in FOWA for (A) $k_s = 1 \times 10^4$ cm s^{-1} and (B) $k_s = 0.1$ cm s^{-1}. ECEC Model: $E_1 - E_2 = -0.5$ V, $k_2 = 100$ s^{-1}, $\upsilon = 0.05$ V s^{-1}, $D = 1 \times 10^{-5}$ cm^2 s^{-1}.

Applying the Electrochemical Methods to 1. In order to apply the above analyses to voltammograms of **1**, the degree to which the ECEC and EECC mechanisms contribute to the observed catalytic wave must be better understood. Digital simulation was used as an initial assessment of the competition between the ECEC and EECC pathways (Figure 6A) using the experimentally observed potentials of the Ni(II/I) (−0.83 V) and Ni(I/0) (−1.03 V) couples. Simulation of the full model

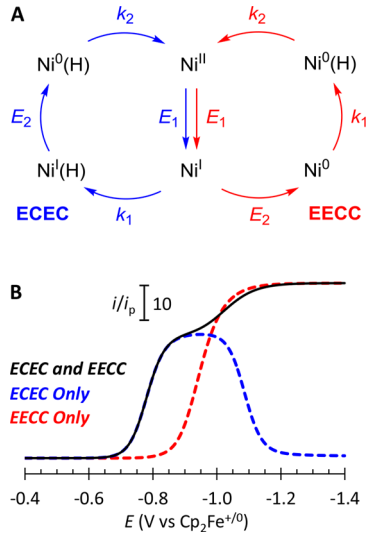

Figure 6. (A) Simulation model for competing ECEC and EECC pathways and (B) simulated voltammograms for the competing ECEC and EECC pathways (black trace), isolated ECEC pathway (dashed blue trace), and isolated EECC pathway (dashed red trace). ECEC model: $E_1 = -0.83$ V, $E_2 = -0.50$ V, $k_1 = 1 \times 10^4$ s^{-1}, $k_2 = 200$ s^{-1}. EECC model: $E_1 = -0.83$ V, $E_2 = -1.03$ V, $k_1 = 1 \times 10^6$ s^{-1}, $k_2 = 300$ s^{-1}. General parameters: $\upsilon = 0.05$ V s^{-1}, $D = 1 \times 10^{-5}$ cm^2 s^{-1}, $k_s = 0.5$ cm s^{-1}.

DOI: 10.1021/jacs.5b10853
J. Am. Chem. Soc. 2016, 138, 604−616

affords a voltammogram (Figure 6B, black trace) that is similar in appearance to the experimental voltammograms of **1**, suggesting that this model is a reasonable approximation of the relevant catalytic processes. Next the individual reaction pathways were "isolated" by turning off the chemical steps of the opposing mechanism in the simulation. For example, the ECEC pathway was isolated by setting k_1 of the EECC pathway to 0 s^{-1}, while maintaining the Ni(I/0) reduction in the model. Figure 6B shows the simulated voltammograms of the isolated ECEC pathway (dashed blue trace) and the isolated EECC pathway (dashed red trace).

At potentials positive of the Ni(II/I) couple (−0.83 V), the catalytic wave of the isolated ECEC pathway (blue trace) is superimposed over the wave simulated from competing ECEC and EECC mechanisms (black trace). This indicates that the current at the beginning of the catalytic wave arises solely from the ECEC pathway, with little to no contribution from the EECC pathway. The catalytic current of the isolated ECEC wave reaches a plateau approximately halfway between the Ni(II/I) and Ni(I/0) couples and then begins to decrease as the potential becomes more negative. This phenomenon indicates that at sufficiently negative potentials, reduction of Ni(I) by the electrode becomes faster than protonation of Ni(I). Consequently, the catalytic current at the most negative potentials corresponds solely to the EECC pathway, as evidenced by the equivalent plateau regions of the isolated EECC wave (red trace) and the wave for the competing ECEC and EECC pathways (black trace). Similar conclusions were reached in a recent computational microkinetics study of **1**.[22]

Given the above considerations, the maximum i_{cat} value at the catalytic plateau of **1** originates predominantly from an EECC pathway (Figure 7A). This maximum i_{cat} value is typically used to measure the proton reduction activity of many $Ni(P^R{}_2N^{R'}{}_2)_2{}^{2+}$ derivatives,[23,53−57] therefore the k_{obs} values previously reported for these catalysts likely reflect the activity of an EECC pathway. Direct measurement of an accurate i_{cat} value for the ECEC pathway is less straightforward since the plateau region for this pathway is obscured by the rise in current associated with the following EECC pathway. However, $E_{cat/2}$ for the ECEC pathway is readily identified by the potential of the first maximum observed in the first derivative of the i−E trace (Figure 7B).[58] In the cyclic voltammogram, the current at $E_{cat/2}$ is equal to half of i_{cat} by definition (Figure 7A), thus i_{cat} and k_{obs} for the ECEC pathway can be measured in this manner. Additionally, the first derivative trace can be used to approximate the potential at which the EECC begins to compete with the ECEC pathway by reflecting the early portion of the trace through the potential of the first maximum (Figure 7B, dashed blue trace). The resulting reflection does not deviate from the real derivative at potentials positive of the Ni(II/I) couple (−0.83 V), indicating that the EECC pathway does not become kinetically competitive with the ECEC pathway prior to the Ni(II/I) couple.

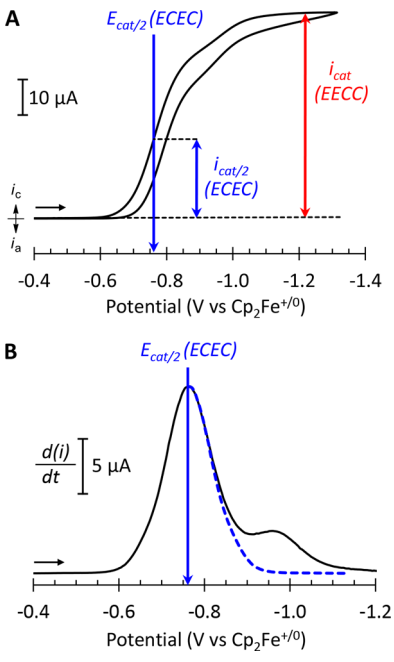

Figure 7. (A) Cyclic voltammogram of **1** showing the methods for measuring i_{cat} and $E_{cat/2}$ for the ECEC and EECC mechanisms, and (B) first-derivative plot of the cyclic voltammogram of **1**, with the dashed blue line illustrating the reflection of the derivative across the potential of the first maximum. Conditions: **1** (0.7 mM) and $DMF(H)^+$ (158 mM) in MeCN (0.2 M NBu_4PF_6), υ = 0.05 V s^{-1}, 1 mm diameter glassy carbon working electrode.

For a given mechanism, k_1 and k_2 can be determined from $E_{cat/2}$ and i_{cat} or by using FOWA as described above. Both of these techniques can be used to examine of the kinetics of the ECEC pathway for **1** by using the value of the Ni(II/I) couple for the noncatalytic reduction potential $E_{1/2}$. More difficult is analysis of the EECC pathway of **1**, as the voltammetric response is perturbed by the preceding ECEC pathway until the catalytic plateau is reached. The second maximum observed at −0.96 V in the first derivative plot does not provide $E_{cat/2}$ for the EECC pathway, but instead identifies the potential at which the catalyst has an equal chance of entering either an ECEC or an EECC pathway. Therefore, the present electrochemical analysis cannot be used to experimentally determine the k_1 and k_2 values of the EECC pathway of **1** when both the ECEC and EECC pathways are operative.

Acid and Base Dependence of Electrocatalytic Proton Reduction by 1. Understanding the acid and base dependence of k_{obs} for the individual ECEC and EECC pathways is a crucial step for gaining mechanistic insights into the catalytic production of H_2. Cyclic voltammograms of **1** were recorded in acetonitrile solution (0.2 M NBu_4PF_6 electrolyte) in the presence of 0.005−0.25 M of $DMF(H)^+$, 1:3 DMF:$DMF(H)^+$, and 1:1 DMF:$DMF(H)^+$. The value for k_{obs} of each pathway was determined from the corresponding i_{cat} value, measured either from the plateau-limiting current (EECC) or from twice the current at the potential of the first maximum in the first derivative trace (ECEC). The resulting plots of k_{obs} versus concentration of $DMF(H)^+$ are shown for both the ECEC pathway (Figure 8A) and the EECC pathway (Figure 8B). The EECC pathway is clearly faster than the ECEC pathway under similar conditions. However, as noted previously,[23] **1** displays slower rates of catalysis for both pathways when using buffered DMF:$DMF(H)]^+$ mixtures. This observation is counterintuitive since base is required to deprotonate the exo-protonated intermediates that are believed to inhibit catalytic formation of H_2.[28] We address this discrepancy next by considering the effect of homoconjugation.

In the homoconjugation reaction, an acid and its conjugate base react to form a hydrogen-bonded pair (eq 10). Proper treatment of this phenomonenon is essential for understanding the kinetics of protonation of **1** (and related catalysts) since a homoconjugation constant (K_f) of 49 M^{-1} has been measured

DOI: 10.1021/jacs.5b10853
J. Am. Chem. Soc. 2016, 138, 604−616

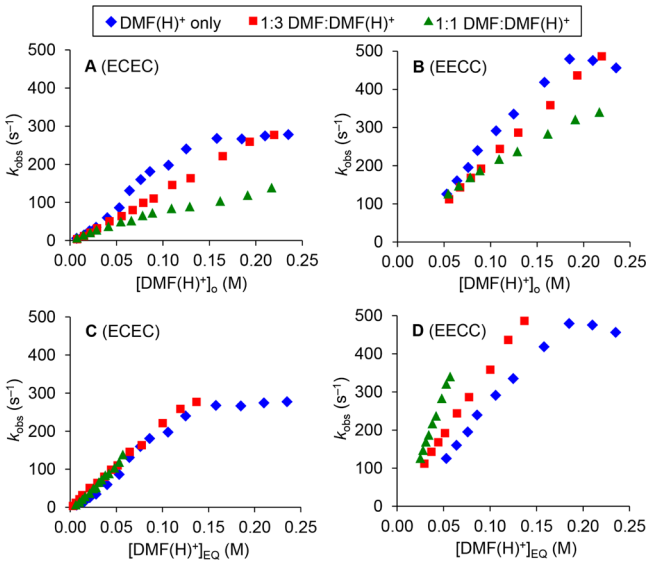

Figure 8. Plots of k_{obs} versus acid concentration. (A) ECEC, $[DMF(H)^+]_o$ (uncorrected for homoconjugation), (B) EECC, $[DMF(H)^+]_o$ (uncorrected for homoconjugation), (C) ECEC, $[DMF(H)^+]_{EQ}$ (corrected for homoconjugation), and (D) EECC, $[DMF(H)^+]_{EQ}$ (corrected for homoconjugation).

for $DMF(H)^+$ in acetonitrile.[59] A critical question is whether the homoconjugate pair is capable of directly protonating or deprotonating the catalytic intermediates. For the present case, $(DMF)_2(H)^+$ is a poorer acid than $DMF(H)^+$ on the basis of thermodynamic and steric considerations and is therefore unlikely to directly protonate the Ni intermediates. Similarly, we will assume that $(DMF)_2(H)^+$ does not play a significant role as a base. The equilibrium concentration of the monomeric acid in solution, $[BH^+]_{EQ}$, can be determined from the initial concentrations of acid and base ($[BH^+]_o$ and $[B]_o$) and the homoconjugation constant (K_f), according to eq 11. A similar equation can be written to determine $[B]_{EQ}$, the concentration of monomeric base in solution (eq 12). Therefore, the homoconjugation reaction serves to decrease the concentrations of $DMF(H)^+$ and DMF (the substrates) in solution (Figure S2), and the kinetics for electrocatalysis must account for this phenomenon.

$$BH^+ + B \rightleftharpoons BHB^+ \quad K_f \tag{10}$$

$$[BH^+]_{EQ} = \frac{-\{K_f([B]_o - [BH^+]_o) + 1\} + \sqrt{\{K_f([B]_o - [BH^+]_o) + 1\}^2 + 4K_f[BH^+]_o}}{2K_f} \tag{11}$$

$$[B]_{EQ} = \frac{-\{K_f([BH^+]_o - [B]_o) + 1\} + \sqrt{\{K_f([BH^+]_o - [B]_o) + 1\}^2 + 4K_f[B]_o}}{2K_f} \tag{12}$$

Returning to the acid dependence of **1**, the plots of k_{obs} versus $[DMF(H)^+]_o$ (Figure 8A,B) can be converted into plots of k_{obs} versus $[DMF(H)^+]_{EQ}$ (Figure 8C,D). After correcting the acid concentration for homoconjugation in the buffered solutions, k_{obs} is linear with respect to the acid concentration under the range of acid concentrations examined. Catalysis is also first-order in acid at low concentrations of $DMF(H)^+$ with no buffer, but becomes independent of the acid concentration at ~0.2 M $DMF(H)^+$.[23] Notably, correction of the acid concentrations due to homoconjugation reveals that k_{obs} of the ECEC pathway is independent of the base concentration, while k_{obs} of the EECC pathway increases in the presence of added base. The latter finding for the EECC pathway is consistent with an increased rate of isomerization from exo to endo-protonated species in the presence of added base.

The absence of a base concentration dependence of k_{obs} for the ECEC pathway was further examined through determination of k_1 and k_2 from the $E_{cat/2}$ values (Tables S1–S3). Second-order rate constants were measured from plots of the pseudo-first-order rate constants versus $[DMF(H)^+]_{EQ}$ (Figures S7–S9) and are listed in Table 2.[60] A large k_1 value of

Table 2. Second-Order Rate Constants (M^{-1} s^{-1}) for Electrocatalytic Hydrogen Production by 1 Measured by $E_{cat/2}$ Analysis

		BH^{+a}	1:3 B:BH^+	1:1 B:BH^+
ECEC	k_1	330,000	120,000	14,000
	k_2	2300	3000	6900
	k_{obs}	1900	2100	2200
EECC	k_{obs}	2600	3600	5700

[a]Rate constants measured from the linear region prior to acid saturation.

330,000 M^{-1} s^{-1} was measured using unbuffered $DMF(H)^+$ and was found to decrease by two-thirds using 1:3 DMF:$DMF(H)^+$ (k_1 = 120,000 M^{-1} s^{-1}) and over an order of magnitude with 1:1 DMF:$DMF(H)^+$ (k_1 = 14,000 M^{-1} s^{-1}). This finding indicates that the protonated Ni(I) intermediate is readily deprotonated in the presence of added base, leading to a slower net rate of protonation. In contrast to k_1, a 3-fold increase in k_2 is observed upon moving from unbuffered $DMF(H)^+$ to 1:1 DMF:$DMF(H)^+$. In the presence of a 1:1 buffer, k_1 (14,000 M^{-1} s^{-1}) is only 2-fold larger than k_2 (6900 M^{-1} s^{-1}), which implies that both steps contribute to the observed catalytic rate since k_{obs} (2200 M^{-1} s^{-1}) is smaller than either of the individual rate constants. Thus, there is a trade-off for the ECEC pathway, where added base facilitates the second catalytic step but hinders the first.

Unlike the ECEC pathway, an accurate $E_{cat/2}$ for the EECC path of **1** cannot be identified under these conditions, due to the transition from an ECEC to EECC mechanism. However, an approximate kinetic analysis of the EECC pathway indicates that the second chemical step is rate-determining for catalysis (see SI). A similar conclusion was reached by Dempsey et al. in studies of **1** using a much weaker acid, anilinium (pK_a = 10.6),[61] where catalysis through the ECEC pathway is negligible.[29] Therefore, k_{obs} can be approximated to be equal to k_2 for the EECC pathway of **1**.

FOWA of ECEC Pathway. FOWA was performed on **1** using $E_{1/2}$ = −0.83 V (the potential of the Ni(II/I) couple) and i/i_p values up to 3% of the maximum i_{cat}/i_p of the ECEC pathway. The ratio of the k_1 values determined from $E_{cat/2}$ analysis and FOWA were plotted versus $[DMF(H)^+]_{EQ}$ (Figure 9A). Under buffered conditions, the k_1 values measured from $E_{cat/2}$ analysis were 1.5–3.0 times larger than the values measured by FOWA. This trend is opposite to that expected from simulations and suggests that an unexpected phenomenon is occurring at the foot of the wave.

The behavior at the foot of the wave was further explored by examining the dependence of k_1 on the percent of i_{cat}/i_p used for FOWA of **1** in the presence of 1:1 DMF:$DMF(H)^+$ (Figure 9B). Surprisingly, the value of k_1 was found to increase linearly as the percentage of i_{cat}/i_p used in FOWA was increased from 3% to 20%, while further increases in the percentage of i_{cat}/i_p led to a decrease in k_1. This trend again contradicts the

DOI: 10.1021/jacs.5b10853
J. Am. Chem. Soc. 2016, 138, 604–616

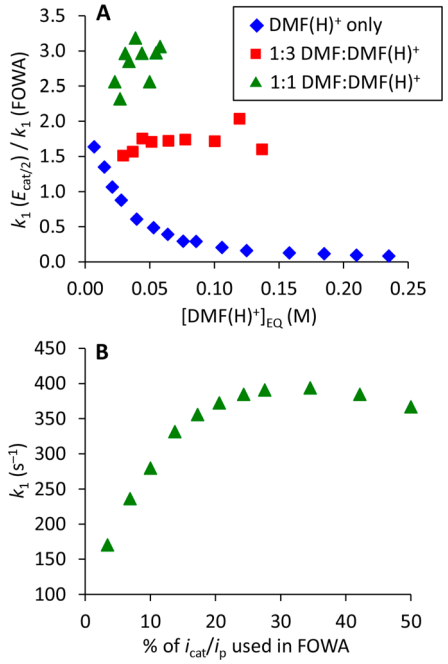

Figure 9. (A) Plot of the ratio of k_1 obtained from $E_{cat/2}$ analysis and FOWA versus $[DMF(H)^+]_{EQ}$, and (B) plot of k_1 versus the percent of i_{cat}/i_p used in the FOWA for $[DMF(H)^+]_{EQ}$ = 57 mM with 1:1 DMF:DMF(H)$^+$.

simulations, which afforded larger k_1 values as less of the wave was used in FOWA (Figure 5). A possible cause of this phenomenon is that the reduction potential of the protonated Ni(I) intermediate lies near the foot of the wave, leading to an increase in current as more of the intermediate is reduced. This hypothesis was tested through simulation of a model ECEC mechanism having E_1 = −0.83 V for the Ni(II/I) couple and E_2 = −0.75 V for reduction of the protonated Ni(I) intermediate. FOWA on the simulated voltammograms of this model led to a qualitative reproduction of the behavior shown in Figure 9b, thus providing support for the hypothesis (Figures S12−S14).

Additionally, FOWA can be used to estimate the reduction potential of the protonated Ni(I) intermediate of the ECEC mechanism. This is accomplished by converting the current axis in Figure 9B into a potential axis, so that the k_1 values obtained from FOWA are plotted versus the most negative potential used in FOWA. The reduction potential of the protonated Ni(I) intermediate is approximately equal to the potential providing the largest k_1 value by FOWA. Simulations can be used to show that this approximation is most appropriate when the kinetic parameter λ is small, i.e., k_1 is not much larger than k_2 (Figures S15−S16). These conditions are met for **1** when using 1:1 DMF:DMF(H)$^+$ as the proton source, and the potential analysis provides a value of −0.79 V for the protonated Ni(I) intermediate (Figure S17).

Thus, far, FOWA of **1** has only been discussed using DMF:DMF(H)$^+$ mixtures as the proton source. When unbuffered DMF(H)$^+$ is employed, the pseudo-first-order k_1 values obtained from FOWA are larger than those obtained from $E_{cat/2}$ analysis at acid concentrations >30 mM (Figure 9A, blue diamonds). Plots of k_1 measured from FOWA versus concentration of DMF(H)$^+$ show two distinct linear regions at low and high acid concentrations (Figures S18−S19). We interpret these data to mean that at the foot of the catalytic wave, increasing the concentration of unbuffered DMF(H)$^+$ causes **1** to transition from an ECEC mechanism to a CECE mechanism involving reduction of a protonated Ni(II) species. However, the CECE pathway does not appear to be operative at more negative potentials, since the k_1 values measured by $E_{cat/2}$ analysis showed a first-order dependence on acid over the entire concentration range of DMF(H)$^+$. For this reason, it is likely that the CECE pathway is only operative at the foot of the wave and that catalytic turnover quickly generates enough DMF in the diffusion layer to deprotonate any protonated Ni(II) species that may be present.

DISCUSSION

Electrocatalytic Mechanism. The proposed electrocatalytic network for production of H_2 by **1** is shown in Scheme 2. Protonation of the catalytic intermediates at the pendant amines forms endo and exo isomers. In the nomenclature of Scheme 2, endo and exo protonation isomers are designated by **e** and **x**, and the formal oxidation state of nickel is given in parentheses. The k_1 and k_2 rate constants for both the ECEC and EECC pathways are global rate constants comprising multiple chemical steps. For the ECEC pathway, both endo and exo protonation

Scheme 2. Proposed Catalytic Cycle for Electrocatalytic Production of H_2 by 1[a]

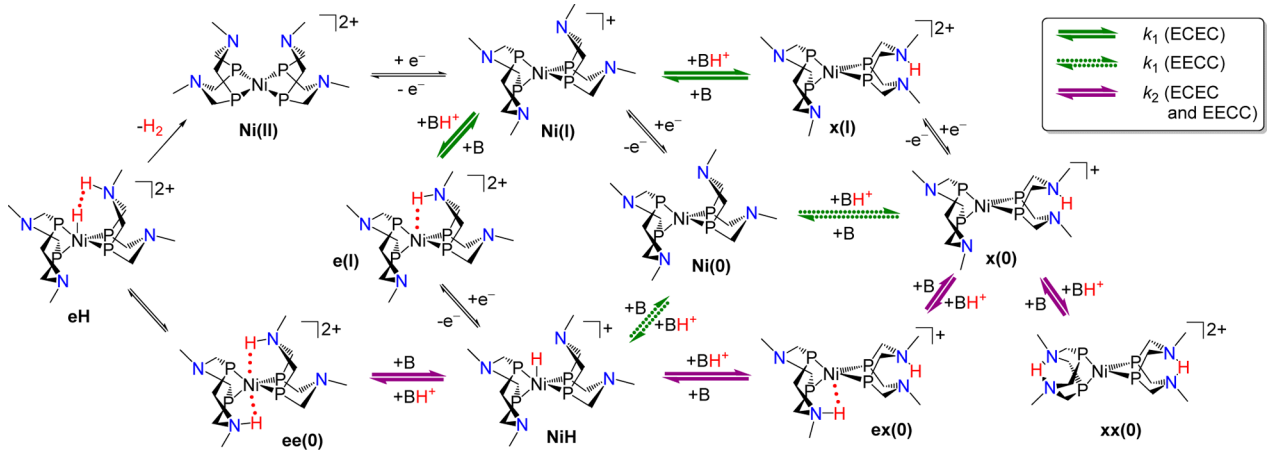

[a]The Ph groups on P and N have been omitted for clarity.

DOI: 10.1021/jacs.5b10853
J. Am. Chem. Soc. 2016, 138, 604−616

of Ni(I) can potentially contribute to k_1 (solid green arrows), while endo and exo protonation of Ni(0) can affect k_1 of the EECC pathway (dashed green arrows). The ECEC and EECC pathways share a common set of steps corresponding to k_2, namely protonation to form doubly protonated Ni(0) species and subsequent isomerization to the **ee(0)** isomer (purple arrows). In principal elimination of H_2 from the **ee(0)** isomer could also contribute to the measured k_2 values. However, turnover frequencies as high as 5×10^5 s^{-1} have been measured for **1** in protic ionic liquids,[25,26] indicating that H_2 elimination is much faster than the turnover frequencies observed under the present conditions (<500 s^{-1}).

Despite being unsuitable for accurate kinetic measurements under these conditions, FOWA afforded valuable mechanistic insight on the intermediate(s) formed under electrocatalytic conditions. Using FOWA, a reduction potential of −0.79 V was estimated for the singly protonated Ni(I) intermediate. This potential is 250 mV more positive than the Ni(I/0) couple of **1** ($E_{1/2}$ = −1.03 V), and comparisons to related complexes suggest that this species is the exo-protonated isomer, **x(I)**, rather than the endo-protonated isomer, **e(I)**. Recent studies on $Ni^{I}(P^{tBu}_2N^{Bn}_2)_2^+$ demonstrated that reduction of **e(I)** occurs approximately 400 mV more positive than the corresponding Ni(I/0) couple.[62] Applying this relationship to **1** allows one to estimate a reduction potential of −0.63 V for the **e(I)** isomer of **1**, which is approximately 100 mV more positive than the foot-of-the-wave region observed for **1** with 1:1 DMF:DMF(H)$^+$ and implies the **e(I)** isomer is not significantly populated under these conditions. Mono-exo Ni(I) or Ni(0) species have not been observed experimentally; however, the **xx(0)** isomer of the related complex $Ni^0(P^{tBu}_2N^{Bn}_2\text{-}H)_2^{2+}$ displays a quasi-reversible oxidation that is 680 mV positive of the Ni(I/0) couple as a result of electrostatic and inductive effects.[63] A reasonable estimate of the singly protonated **x(0)** complex would be that it is oxidized 340 mV positive of the Ni(I/0) couple, which is close to the experimentally observed difference of 240 mV for **1**, providing support for this structural assignment.

For the ECEC pathway, FOWA analysis indicates that exo protonation of Ni(I) is kinetically preferred over endo protonation, as observed in prior spectroscopic studies of other doubly protonated $Ni^0(P^R_2N^{R'}_2\text{-}H)_2^{2+}$ complexes.[28,32] This finding differs from a recent computational microkinetics study of **1**, which estimated the free-energy barrier for protonation of Ni(I) in an endo position is 2 kcal mol^{-1} lower than for the exo position.[22] Despite this minor discrepancy, both the microkinetics study and the present findings demonstrate that exo protonation at Ni(I) impedes catalytic turnover due to accumulation of exo-protonated Ni(0) isomers in the diffusion layer. This conclusion is supported by the 3-fold increase in k_2 for the ECEC pathway upon switching from DMF(H)$^+$ to 1:1 DMF:DMF(H)$^+$ as the acid, corresponding to an increased rate of exo to endo isomerization of the doubly protonated Ni(0) intermediates in the presence of added base.

A k_1 value for the EECC pathway could not be measured due to interference from the preceding ECEC pathway, but was estimated to be significantly larger than k_{obs} (see SI). In a complementary study of **1** using anilinium as the proton source, Dempsey et al. measured a k_1 value (6.5×10^6 M^{-1} s^{-1}) that is approximately 5 orders of magnitude larger than k_{obs} (~50 M^{-1} s^{-1}) for the EECC pathway.[29] Information on the endo versus exo regioselectivity of Ni(0) protonation cannot be obtained from the magnitude of k_1, but can be inferred from comparison of the k_2 values measured for the ECEC and EECC pathways. While the catalytic steps corresponding to k_2 appear to be identical for both mechanisms, the measured k_2 values could be significantly different if Ni(0) has a greater probability to be protonated in an endo position than Ni(I). Comparison of the measured k_2 values, approximated as k_{obs} for the EECC pathway, does not reveal a significant difference between the two mechanisms (Table 2). Therefore, the first chemical step of the EECC pathway for **1** is most likely exo protonation of Ni(0), similar to the ECEC pathway in which Ni(I) is protonated in an exo position.

Catalytic Tafel Plots. In general terms, overpotential (η) for the electrocatalytic production of H_2 is the difference between the potential of catalysis (E) and the thermodynamic potential of the H^+/H_2 couple (E_{H^+}) under the specific reaction conditions (eqs 13 and 14). The potential at which catalysis occurs for molecular electrocatalysts is traditionally reported using $E_{cat/2}$, where the turnover frequency (TOF) is equal to $0.5 \times k_{obs}$.[46] FOWA has recently been suggested as an improved method for analyzing η in molecular electrocatalysis.[51,52,64] The FOWA equations can be adapted to obtain a "catalytic Tafel plot" (eq 15), where the TOF is described as a function of the amount of catalyst that is reduced at a given overpotential. The turnover frequency at zero overpotential (TOF_o, eq 16) is obtained when $\eta = 0$ in eq 15. For a given catalyst, TOF_o is no more significant than TOF at $E_{cat/2}$ since the two are linked on the overpotential axis by a common slope of f/ln 10. However, use of TOF_o does simplify the comparison between different catalysts, as the TOF−η landscape is reduced to a single dimension (TOF) at $\eta = 0$.[64]

$$\eta = E_{H^+} - E \tag{13}$$

$$E_{H^+} = E^{\circ}_{H^+} + \frac{RT}{nF}\ln\frac{K_a[BH^+]}{P_{H_2}[B]} \tag{14}$$

$$TOF = \frac{k_{obs}}{1 + \exp[f(E_{H^+} - \eta - E_{cat/2})]} \tag{15}$$

$$TOF_o = \frac{k_{obs}}{1 + \exp[f(E_{H^+} - E_{cat/2})]} \tag{16}$$

Artero and Savéant reported catalytic Tafel plots for **1** and several related complexes[64] using kinetic data from the literature that did not account for the competing ECEC and EECC mechanisms.[23,24] Here we examine the TOF−η plots for the different mechanisms of **1** in the presence of 185 mM DMF(H)$^+$, which provides the limiting k_{obs} values for this acid (Figure 8). In keeping with common practice, E_{H^+} is defined by assuming [DMF(H)$^+$] = [DMF] and P_{H_2} = 1 atm.[46] A value of E_{H^+} = −0.50 V was used by Artero and Savéant[64] based on a method for estimating E_{H^+} for acids that homoconjugate.[58] However, we use the more accurate value of E_{H^+} = −0.38 V, which was measured directly for 1:1 DMF:DMF(H)$^+$ using equilibrium open circuit potential measurements that inherently account for homoconjugation.[59] Values of $E_{cat/2}$ for the ECEC (−0.76 V) and EECC (−0.96 V) pathways were measured from the two maxima observed in the $d(i)/dt$−E trace (illustrated in Figure 7b), and the resulting Tafel plots are shown in Figure 10.

The transition from the ECEC pathway to the EECC pathway is accompanied by an increase in both k_{obs} and in the overpotential, as the EECC pathway occurs at more negative potentials than the ECEC path. TOF_o for the two mechanisms

DOI: 10.1021/jacs.5b10853
J. Am. Chem. Soc. 2016, 138, 604−616

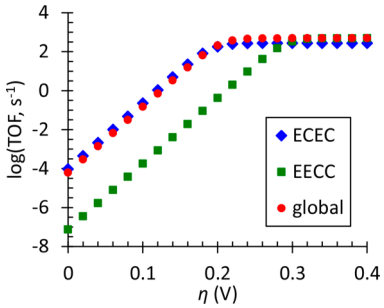

Figure 10. Catalytic Tafel plots for **1** in the presence of 185 mM $DMF(H)^+$ using E_{H^+} = −0.38 V. ECEC: $E_{cat/2}$ = −0.76 V, k_{obs} = 270 s^{-1}; EECC: $E_{cat/2}$ = −0.96 V, k_{obs} = 480 s^{-1}; global: $E_{cat/2}$ = −0.79 V, k_{obs} = 480 s^{-1}.

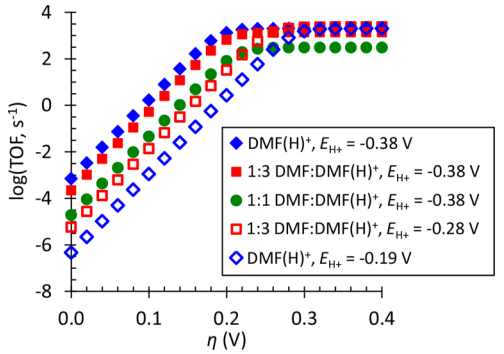

Figure 11. Catalytic Tafel plots for the ECEC mechanism of **1** with different ratios of DMF:$DMF(H)^+$ (1 M H^+) and different values of E_{H^+}.

of **1** differs by about three orders of magnitude, indicating that the ECEC pathway is more efficient than the EECC pathway. The kinetic analysis described above reveals that the difference in k_{obs} between the two mechanisms is due primarily to the greater rate of exo protonation of Ni(0) compared to Ni(I). This trend is most likely due to an increase in the basicity of the pendant amines upon reduction from Ni(I) to Ni(0).[63] DFT calculations support this interpretation, as the computed pK_a of **x(0)** (10.9) is greater than **x(I)** (5.5).[22] Therefore, the TOF of **1** is fundamentally connected to η by the thermodynamic properties of the intermediates along the ECEC and EECC pathways.

A third Tafel plot (Figure 10, red dots) was generated using the global analysis that is traditionally reported for **1** and related complexes. In the global analysis, k_{obs} is measured from i_{cat} and corresponds to the EECC mechanism, and $E_{cat/2}$ is measured at half of i_{cat}, providing a potential where both the ECEC and EECC mechanisms are occurring. The catalytic Tafel plot generated from the global analysis is nearly identical to the plot for the ECEC mechanism (Figure 10), which suggests that it is reasonable to generate catalytic Tafel plots for other $Ni(P^R{}_2N^{R'}{}_2)_2{}^{2+}$ complexes using previously reported data.

Benchmarking studies are ideally conducted under identical reaction conditions to obtain the most meaningful comparisons of different catalysts.[65] This presents a challenge for comparison of molecular electrocatalysts since a wide range of reaction conditions are commonly employed. Artero and Savéant have proposed reporting catalytic Tafel plots at 1 M acid concentration as a means to improve the comparison of molecular H_2 production electrocatalysts,[64] and several catalyst studies have adopted this approach.[66−68] In principle, this convention is a good idea, but unfortunately its implementation leads to the use of several assumptions that might limit the accuracy of data reported in this manner. These considerations are examined below using **1** as an illustrative example, with data tabulated in Table 3 and catalytic Tafel plots displayed in Figure 11.

Kinetic data for H_2 production are often measured at low concentrations of acid (<0.1 M) and extrapolated to 1 M acid.[64] This practice can be problematic since it precludes the possibility of saturation kinetics that would limit the TOF at acid concentrations less than 1 M. As an example, the TOF for **1** is first-order in $[DMF(H)^+]$ at low acid concentrations, but becomes independent of the acid concentration at $[DMF(H)^+]$ ∼ 0.19 M. Extrapolation from the low acid concentration regime to 1 M $DMF(H)^+$ provides a TOF of 1900 s^{-1}, which is 7× larger than the maximum TOF of 270 s^{-1} observed in the acid-saturation regime. This difference in rates also translates to the TOF_o values measured from a catalytic Tafel analysis. Therefore, the catalytic performance of **1** is *overestimated* by extrapolating the TOF from low acid concentrations to 1 M acid. Similar effects could be important for other catalysts, but are typically not reported.

Another concern is that the value used for E_{H^+} frequently does not reflect the actual solution conditions in the electrochemical diffusion layer. Molecular electrocatalysts for hydrogen production are commonly studied in organic solvents using an organic acid with no added conjugate base and no dihydrogen. The conventional approach for determining E_{H^+} is to assume that half of the acid substrate is consumed at $E_{cat/2}$, which permits ready estimation of E_{H^+} from $E^\circ_{H^+}$ and the pK_a of the acid since $[BH^+]$ = [B] and P_{H_2} = 1 atm (i.e., a solution saturated in H_2).[46,58] However, this assumption does not accurately represent the conditions present at the foot-of-the-wave or for a canonical S-shaped catalytic wave, since consumption of acid within the diffusion layer is minimal in each of these kinetic regimes.[51,69] The errors introduced by the assumption of a 1:1 buffer could be minimal if catalysis is unaffected by

Table 3. Parameters for Generating Catalytic Tafel Plots for the ECEC Mechanism of 1 at 1 M H^+

conditions	$[DMF(H)^+]_o$ (M)	$[DMF]_o$ (M)	$[DMF(H)^+]_{EQ}$ (M)	$[DMF]_{EQ}$ (M)	E_{H^+} (V)	$E_{cat/2}$ (V)	TOF[a] (s^{-1})	log(TOF_o)
acid only	0.19	0	0.19	0	−0.38[b]	−0.76	270	−4.0
	1.0	0	1.0	0	−0.38[b]	−0.76	1900	−3.2
	1.0	0	1.0	0	−0.19[c]	−0.76	1900	−6.3
1:3 buffer	1.0	0.33	0.66	0.01	−0.38[b]	−0.78	1400	−3.7
	1.0	0.33	0.66	0.01	−0.28[d]	−0.78	1400	−5.3
1:1 buffer	1.0	1.0	0.13	0.13	−0.38	−0.81	300	−4.7

[a]Determined from k_{obs} (M^{-1} s^{-1}, Table 2) and $[DMF(H)^+]_{EQ}$. [b]Using the value for 1:1 buffer as an estimate. [c]Open circuit value determined according to method of Roberts and Bullock (ref 59). [d]Obtained from substituting $[DMF(H)^+]_{EQ}$ and $[DMF]_{EQ}$ into eq 14 assuming P_{H_2} = 1 atm.

DOI: 10.1021/jacs.5b10853
J. Am. Chem. Soc. 2016, 138, 604−616

either H_2 or conjugate base, but this is not typically reported for most catalysts.

The findings reported here for **1** can be used to highlight several ways that a catalytic Tafel plot might be affected by different ratios of acid and base. Tafel plots for the ECEC mechanism of **1** at 1 M acid were generated for the different ratios of DMF:DMF(H)$^+$ using the common approximation that E_{H^+} is identical to the value for a 1:1 buffer under all conditions (Figure 11). The Tafel plot for unbuffered DMF(H)$^+$ (solid blue diamonds) was obtained by extrapolation from low acid concentrations, as described above. Some of the monomeric acid is trapped in the homoconjugate pair under buffered conditions, resulting in a concentration of DMF(H)$^+$ that is less than 1 M (Table 3). Consequently, the catalytic Tafel plots for 1:3 DMF:DMF(H)$^+$ (solid red squares) and 1:1 DMF:DMF(H)$^+$ (solid green circles) display maximum TOF values that are lower than observed for unbuffered DMF(H)$^+$. Additionally, $E_{cat/2}$ for the ECEC pathway shifts to more negative potentials in the presence of base, which causes a shift of the entire Tafel plot to higher η under buffered conditions. The net result of these effects, when using a common value of E_{H^+}, is that TOF_o decreases by approximately 30-fold upon moving from 1 M of unbuffered DMF(H)$^+$ to 1:1 DMF:DMF(H)$^+$.

Since the presence of base clearly affects the kinetics of H_2 production by **1**, more accurate determinations of E_{H^+} will provide more meaningful Tafel plots. A value of P_{H_2} = 1 atm can be assumed since the catalytic response of **1** is known to be unaffected by performing catalysis under an atmosphere of H_2.[59] Therefore, E_{H^+} for 1:1 DMF:DMF(H)$^+$ remains unchanged, and E_{H^+} for 1:3 DMF:DMF(H)$^+$ at 1 M H^+ is readily determined to be −0.28 V using eq 14 and the concentrations of monomeric acid and base. A value of E_{H^+} for unbuffered DMF(H)$^+$ cannot be estimated from eq 14 due to the absence of conjugate base. However, open circuit potential measurements performed on acetonitrile solutions of unbuffered DMF(H)$^+$ under an atmosphere of H_2 were found to display a logarithmic dependence on the concentration of DMF(H)$^+$, which allows a value of E_{H^+} = −0.19 V to be estimated for 1 M DMF(H)$^+$.[59]

These corrections to E_{H^+} afford revised Tafel plots for 1:3 DMF:DMF(H)$^+$ (open red squares) and unbuffered DMF(H)$^+$ (open blue diamonds) as shown in Figure 11. Notably, accurate determination of E_{H^+} causes a reversal in the ordering of TOF_o for the different buffer conditions, with TOF_o increasing approximately 40-fold by switching from unbuffered DMF(H)$^+$ to 1:1 DMF DMF:DMF(H)$^+$. Perhaps most significant is the observation that the TOF_o for **1** is overestimated by 3 orders of magnitude when using the conventional assumption of buffered conditions for determination of E_{H^+} with catalytic data obtained using unbuffered DMF(H)$^+$. These findings suggest that greater care is required in reporting accurate TOF_o values for meaningful catalyst benchmarking.

CONCLUSIONS

We have reported a detailed kinetic analysis on electrocatalytic proton reduction by $Ni(P^{Ph}_2N^{Ph}_2)_2^{2+}$ (**1**) using recent methodologies developed by Costentin and Savéant. The presence of competing ECEC and EECC mechanisms complicates the kinetic analysis, but with the aid of digital simulations, a strategy was developed to measure the catalytic rate constant (k_{obs}) for each of the two pathways using the first-derivative plot of the voltammograms. Notably, the EECC pathway results in a larger k_{obs} than the ECEC pathway due to an increased rate of protonation of Ni(0) over Ni(I). FOWA of **1** did not afford accurate rate constants due to competing side-phenomena at the foot-of-the-wave, but allowed for an estimate for the reduction potential of the protonated Ni(I) intermediate, corresponding to the second electron transfer in the ECEC mechanism. Comparison to other $Ni(P^R_2N^{R'}_2)_2^{2+}$ derivatives suggests the Ni(I) intermediate is protonated in an exo position, which is known to be detrimental to catalysis.

The methods detailed here could potentially be implemented in the kinetic analysis of other electrocatalysts capable of operating by multiple mechanisms. Proper kinetic analysis requires careful scrutiny of transitory regions between mechanisms as well as the strengths and limitations of the electrochemical methods employed for the kinetic analysis. The findings in our kinetic analysis of **1**, a catalyst with a well-understood mechanism, provide an initial foundation for analysis of other electrocatalysts displaying complex mechanisms.

EXPERIMENTAL SECTION

Materials. Acetonitrile (Alfa-Aesar, anhydrous, amine-free) and dimethylformamide (Burdick & Jackson) were purified by sparging with N_2 and passage through neutral alumina. Tetrabutylammonium hexafluorophosphate (Fluka, ≥ 99%) was used as received. Ferrocene (Aldrich) was purified by sublimation under vacuum before use. Dimethylformamide-trifluoromethanesulfonic acid, [DMF(H)](OTf),[70] and **1**[24] were prepared using published procedures.

Instrumentation. Voltammetry measurements were performed using a CH Instruments 620D potentiostat equipped with a standard three-electrode cell. Experiments were performed in a nitrogen-filled glovebox at ambient temperature, 23 ± 2 °C, using a 3−5 mL conical glass vial fitted with a polysilicone cap having openings sized to closely accept each electrode. The working electrode was a 1 mm PEEK-encased glassy carbon disc (Cypress Systems EE040), the counter electrode was a glassy carbon rod (Structure Probe, Inc.), and the pseudoreference electrode was a silver wire suspended in a solution of NBu_4PF_6 (0.2 M) in acetonitrile and separated from the analyte solution by a Vycor frit (CH Instruments 112). The working electrode was polished with diamond paste (Buehler, 0.25 μm) on a polishing pad wet with H_2O, then the electrode was rinsed with neat acetonitrile. Ferrocene was used as an internal standard, and all potentials are referenced to the ferrocenium/ferrocene couple at 0 V.

The uncompensated solution resistance (R_u) under these conditions was determined to be <50 Ω using the built-in *iR* compensation feature of the potentiostat. *iR* compensation was not performed in the collection of catalytic data since R_u is small relative to the current measured at $E_{cat/2}$ (<20 μA). The maximum potential error resulting from uncompensated resistance is ∼1 mV, which is smaller than the standard deviation of ±5 mV in the measured $E_{cat/2}$ values.

Electrochemical simulations were performed using DigiElch 7.F. The electrode surface area was set to 0.008 cm^2, υ was set to 0.05 V s^{-1}, and a diffusion coefficient of 1 × 10^{-5} cm^2 s^{-1} was used for all species. Electron transfer was modeled using Butler−Volmer kinetics with α = 0.5 and variable values of k_s. Steady-state catalytic conditions were modeled using irreversible pseudo-first-order chemical reactions (units of s^{-1}).

Catalytic Hydrogen Production. In a representative experiment, **1** (2.2 mg, 0.002 mmol) was dissolved in 2.0 mL of acetonitrile (0.2 M NBu_4PF_6) to afford a 1 mM solution of **1**. Ferrocene was added as an internal reference, and an initial voltammogram was recorded at υ = 0.05 V s^{-1}. Aliquots of a 1.5 M DMF(H)$^+$ solution in acetonitrile (0.2 M NBu_4PF_6) were added via microsyringe in 20−160 μL increments. After each addition of acid, the working electrode was cleaned by polishing and a voltammogram recorded (υ = 0.05 V s^{-1}). For each voltammogram, i_{pa} of the $Cp_2Fe^{+/0}$ oxidation wave was used as an internal reference to adjust i_p and [acid] for sample dilution.

DOI: 10.1021/jacs.5b10853
J. Am. Chem. Soc. 2016, 138, 604−616

Currents were measured by extension from the background capacitive current, which was much smaller than the catalytic current due to the low scan rate. Background subtraction was not employed in FOWA, resulting in a positive nonzero intercept ($\leq$0.15). At lower acid concentrations, the catalytic waves displayed a slight peak shape indicative of substrate depletion, affording a smaller value of i_{cat} than would be expected from a steady-state catalytic plateau. A corrected i_{cat} was measured for these data points by (1) finding the current at the potential of the second maximum in the first derivative trace, which is the point at which half the catalyst operates by ECEC and half by EECC, (2) subtracting the current due to the ECEC process ($0.5 \times i_{cat}^{ECEC}$), and (3) multiplying the remaining current by two.

■ ASSOCIATED CONTENT

Supporting Information

The Supporting Information is available free of charge on the ACS Publications website at DOI: 10.1021/jacs.5b10853.

Algebraic derivations of kinetic expressions, details of acid homoconjugation, cyclic voltammograms, kinetic plots (PDF)

■ AUTHOR INFORMATION

Corresponding Author

*eric.wiedner@pnnl.gov

Notes

The authors declare no competing financial interest.

■ ACKNOWLEDGMENTS

We thank Eric Rountree and Prof. Jillian Dempsey for helpful discussions. This research was supported as part of the Center for Molecular Electrocatalysis, an Energy Frontier Research Center funded by the U.S. Department of Energy, Office of Science, Office of Basic Energy Sciences. Pacific Northwest National Laboratory is operated by Battelle for the U.S. Department of Energy.

■ REFERENCES

(1) Cook, T. R.; Dogutan, D. K.; Reece, S. Y.; Surendranath, Y.; Teets, T. S.; Nocera, D. G. *Chem. Rev.* **2010**, *110*, 6474−6502.
(2) Simmons, T. R.; Berggren, G.; Bacchi, M.; Fontecave, M.; Artero, V. *Coord. Chem. Rev.* **2014**, *270*−*271*, 127−150.
(3) Thoi, V. S.; Sun, Y.; Long, J. R.; Chang, C. J. *Chem. Soc. Rev.* **2013**, *42*, 2388−2400.
(4) Benson, E. E.; Kubiak, C. P.; Sathrum, A. J.; Smieja, J. M. *Chem. Soc. Rev.* **2009**, *38*, 89−99.
(5) Costentin, C.; Robert, M.; Savéant, J. M. *Chem. Soc. Rev.* **2013**, *42*, 2423−2436.
(6) DuBois, D. L. *Inorg. Chem.* **2014**, *53*, 3935−3960.
(7) Savéant, J. M. *Chem. Rev.* **2008**, *108*, 2348−2378.
(8) Rountree, E. S.; McCarthy, B. D.; Eisenhart, T. T.; Dempsey, J. L. *Inorg. Chem.* **2014**, *53*, 9983−10002.
(9) Costentin, C.; Savéant, J. M. *ChemElectroChem* **2014**, *1*, 1226−1236.
(10) Savéant, J. M. *Elements of Molecular and Biomolecular Electrochemistry: An Electrochemical Approach to Election Transfer Chemistry*; Wiley: Hoboken, NJ, 2006.
(11) Nippe, M.; Khnayzer, R. S.; Panetier, J. A.; Zee, D. Z.; Olaiya, B. S.; Head-Gordon, M.; Chang, C. J.; Castellano, F. N.; Long, J. R. *Chem. Sci.* **2013**, *4*, 3934−3945.
(12) Rose, M. J.; Gray, H. B.; Winkler, J. R. *J. Am. Chem. Soc.* **2012**, *134*, 8310−8313.
(13) Roy, S.; Groy, T. L.; Jones, A. K. *Dalton Trans.* **2013**, *42*, 3843−3853.
(14) Capon, J.-F.; Ezzaher, S.; Gloaguen, F.; Pétillon, F. Y.; Schollhammer, P.; Talarmin, J. *Chem. - Eur. J.* **2008**, *14*, 1954−1964.
(15) Manbeck, G. F.; Muckerman, J. T.; Szalda, D. J.; Himeda, Y.; Fujita, E. *J. Phys. Chem. B* **2015**, *119*, 7457−7466.
(16) Carroll, M. E.; Barton, B. E.; Rauchfuss, T. B.; Carroll, P. J. *J. Am. Chem. Soc.* **2012**, *134*, 18843−18852.
(17) White, T. A.; Maji, S.; Ott, S. *Dalton Trans.* **2014**, *43*, 15028−15037.
(18) Kaur-Ghumaan, S.; Schwartz, L.; Lomoth, R.; Stein, M.; Ott, S. *Angew. Chem., Int. Ed.* **2010**, *49*, 8033−8036.
(19) Bourrez, M.; Steinmetz, R.; Gloaguen, F. *Inorg. Chem.* **2014**, *53*, 10667−10673.
(20) Baffert, C.; Artero, V.; Fontecave, M. *Inorg. Chem.* **2007**, *46*, 1817−1824.
(21) Hu, X. L.; Brunschwig, B. S.; Peters, J. C. *J. Am. Chem. Soc.* **2007**, *129*, 8988−8998.
(22) Ho, M.-H.; Rousseau, R.; Roberts, J. A. S.; Wiedner, E. S.; Dupuis, M.; DuBois, D. L.; Bullock, R. M.; Raugei, S. *ACS Catal.* **2015**, *5*, 5436−5452.
(23) Kilgore, U. J.; Roberts, J. A. S.; Pool, D. H.; Appel, A. M.; Stewart, M. P.; Rakowski DuBois, M.; Dougherty, W. G.; Kassel, W. S.; Bullock, R. M.; DuBois, D. L. *J. Am. Chem. Soc.* **2011**, *133*, 5861−5872.
(24) Wilson, A. D.; Newell, R. H.; McNevin, M. J.; Muckerman, J. T.; Rakowski DuBois, M.; DuBois, D. L. *J. Am. Chem. Soc.* **2006**, *128*, 358−366.
(25) Pool, D. H.; Stewart, M. P.; O'Hagan, M.; Shaw, W. J.; Roberts, J. A. S.; Bullock, R. M.; DuBois, D. L. *Proc. Natl. Acad. Sci. U. S. A.* **2012**, *109*, 15634−15639.
(26) Hou, J.; Fang, M.; Cardenas, A. J. P.; Shaw, W. J.; Helm, M. L.; Bullock, R. M.; Roberts, J. A. S.; O'Hagan, M. *Energy Environ. Sci.* **2014**, *7*, 4013−4017.
(27) Wilson, A. D.; Shoemaker, R. K.; Miedaner, A.; Muckerman, J. T.; DuBois, D. L.; Rakowski DuBois, M. *Proc. Natl. Acad. Sci. U. S. A.* **2007**, *104*, 6951−6956.
(28) O'Hagan, M.; Ho, M.-H.; Yang, J. Y.; Appel, A. M.; Rakowski DuBois, M.; Raugei, S.; Shaw, W. J.; DuBois, D. L.; Bullock, R. M. *J. Am. Chem. Soc.* **2012**, *134*, 19409−19424.
(29) Rountree, E. S.; Dempsey, J. L. *J. Am. Chem. Soc.* **2015**, *137*, 13371−13380.
(30) Izutsu, K. *Acid-Base Disociation Constants in Dipolar Aprotic Solvents*; Blackwell Scientific Publications: Oxford, 1990.
(31) Kolthoff, I. M.; Chantooni, M. K.; Bhowmik, S. *Anal. Chem.* **1967**, *39*, 1627−1633.
(32) Appel, A. M.; Pool, D. H.; O'Hagan, M.; Shaw, W. J.; Yang, J. Y.; Rakowski DuBois, M.; DuBois, D. L.; Bullock, R. M. *ACS Catal.* **2011**, *1*, 777−785.
(33) Smith, S. E.; Yang, J. Y.; DuBois, D. L.; Bullock, R. M. *Angew. Chem., Int. Ed.* **2012**, *51*, 3152−3155.
(34) Chen, S.; Ho, M.-H.; Bullock, R. M.; DuBois, D. L.; Dupuis, M.; Rousseau, R.; Raugei, S. *ACS Catal.* **2013**, *4*, 229−242.
(35) Raugei, S.; DuBois, D. L.; Rousseau, R.; Chen, S.; Ho, M.-H.; Bullock, R. M.; Dupuis, M. *Acc. Chem. Res.* **2015**, *48*, 248−255.
(36) Nicholson, R. S.; Shain, I. *Anal. Chem.* **1964**, *36*, 706−723.
(37) Savéant, J. M.; Vianello, E. *Electrochim. Acta* **1965**, *10*, 905−920.
(38) Savéant, J. M.; Vianello, E. In *Advances in Polarography*; Longmuir, I. S., Ed.; Pergamon Press: Cambridge, U.K., 1960; Vol. *1*, pp 367−374.
(39) Bard, A. J.; Faulkner, L. R. *Electrochemical Methods: Fundamentals and Applications*, 2nd ed.; John Wiley & Sons: Hoboken, NJ, 2001.
(40) Mashkina, E.; Bond, A. M. *Anal. Chem.* **2011**, *83*, 1791−1799.
(41) Costentin, C.; Drouet, S.; Robert, M.; Savéant, J. M. *Science* **2012**, *338*, 90−94.
(42) Swaddle, T. W. *Chem. Rev.* **2005**, *105*, 2573−2608.
(43) Matsuda, H.; Ayabe, Y. *Z. Electrochem.* **1955**, *59*, 494−503.
(44) Nicholson, R. S. *Anal. Chem.* **1965**, *37*, 1351−1355.
(45) Tsierkezos, N.; Ritter, U. *J. Appl. Electrochem.* **2010**, *40*, 409−417.
(46) Felton, G. A. N.; Glass, R. S.; Lichtenberger, D. L.; Evans, D. H. *Inorg. Chem.* **2006**, *45*, 9181−9184.

DOI: 10.1021/jacs.5b10853
J. Am. Chem. Soc. 2016, 138, 604−616

(47) McCarthy, B. D.; Martin, D. J.; Rountree, E. S.; Ullman, A. C.; Dempsey, J. L. *Inorg. Chem.* **2014**, *53*, 8350−8361.
(48) Kneten, K. R.; McCreery, R. L. *Anal. Chem.* **1992**, *64*, 2518−2524.
(49) Rice, R. J.; Pontikos, N. M.; McCreery, R. L. *J. Am. Chem. Soc.* **1990**, *112*, 4617−4622.
(50) Hu, I.-F.; Karweik, D. H.; Kuwana, T. *J. Electroanal. Chem. Interfacial Electrochem.* **1985**, *188*, 59−72.
(51) Costentin, C.; Drouet, S.; Robert, M.; Savéant, J. M. *J. Am. Chem. Soc.* **2012**, *134*, 11235−11242.
(52) Costentin, C.; Drouet, S.; Robert, M.; Savéant, J. M. *J. Am. Chem. Soc.* **2012**, *134*, 19949−19950.
(53) Wiedner, E. S.; Helm, M. L. *Organometallics* **2014**, *33*, 4617−4620.
(54) Stewart, M. P.; Ho, M.-H.; Wiese, S.; Lindstrom, M. L.; Thogerson, C. E.; Raugei, S.; Bullock, R. M.; Helm, M. L. *J. Am. Chem. Soc.* **2013**, *135*, 6033−6046.
(55) Wiese, S.; Kilgore, U. J.; Ho, M.-H.; Raugei, S.; DuBois, D. L.; Bullock, R. M.; Helm, M. L. *ACS Catal.* **2013**, *3*, 2527−2535.
(56) Kilgore, U. J.; Stewart, M. P.; Helm, M. L.; Dougherty, W. G.; Kassel, W. S.; Rakowski DuBois, M.; DuBois, D. L.; Bullock, R. M. *Inorg. Chem.* **2011**, *50*, 10908−10918.
(57) Helm, M. L.; Stewart, M. P.; Bullock, R. M.; Rakowski DuBois, M.; DuBois, D. L. *Science* **2011**, *333*, 863−866.
(58) Fourmond, V.; Jacques, P.-A.; Fontecave, M.; Artero, V. *Inorg. Chem.* **2010**, *49*, 10338−10347.
(59) Roberts, J. A. S.; Bullock, R. M. *Inorg. Chem.* **2013**, *52*, 3823−3835.
(60) The ECEC pathway could involve a solution electron-transfer (SET) step, in which the protonated Ni(I) intermediate is reduced by unprotonated Ni(I) instead of the electrode. In the absence of data supporting the kinetic feasibility of SET, we have neglected this step in our analysis. If the ECEC operates exclusively by SET, then k_{obs} and k_1 will be underestimated by a factor of 2, and k_2 will be overestimated by a factor of 2.
(61) Kaljurand, I.; Kutt, A.; Soovali, L.; Rodima, T.; Maemets, V.; Leito, I.; Koppel, I. A. *J. Org. Chem.* **2005**, *70*, 1019−1028.
(62) Kochem, A.; O'Hagan, M.; Wiedner, E. S.; van Gastel, M. *Chem. - Eur. J.* **2015**, *21*, 10338−10347.
(63) Wiedner, E. S.; Yang, J. Y.; Chen, S. T.; Raugei, S.; Dougherty, W. G.; Kassel, W. S.; Helm, M. L.; Bullock, R. M.; Rakowski DuBois, M.; DuBois, D. L. *Organometallics* **2012**, *31*, 144−156.
(64) Artero, V.; Savéant, J. M. *Energy Environ. Sci.* **2014**, *7*, 3808−3814.
(65) McCrory, C. C. L.; Jung, S.; Ferrer, I. M.; Chatman, S. M.; Peters, J. C.; Jaramillo, T. F. *J. Am. Chem. Soc.* **2015**, *137*, 4347−4357.
(66) Sampson, M. D.; Kubiak, C. P. *Inorg. Chem.* **2015**, *54*, 6674−6676.
(67) Elgrishi, N.; Chambers, M. B.; Fontecave, M. *Chem. Sci.* **2015**, *6*, 2522−2531.
(68) van der Meer, M.; Glais, E.; Siewert, I.; Sarkar, B. *Angew. Chem., Int. Ed.* **2015**, *54*, 13792−13795.
(69) Savéant, J. M.; Su, K. B. *J. Electroanal. Chem. Interfacial Electrochem.* **1984**, *171*, 341−349.
(70) Favier, I.; Duñach, E. *Tetrahedron Lett.* **2004**, *45*, 3393−3395.

DOI: 10.1021/jacs.5b10853
J. Am. Chem. Soc. 2016, 138, 604−616